Supplementary text

Description of the ice flow model

The 3D thermomechanical ice sheet model applied is a first-order approximation of the Stokes-equations adopted from Blatter (1995) by Hubbard (2000, 1999) and is an approach that has been independently used by Marshall et al. (2000) to model the Laurentide ice sheet, Pollard and DeConto (2007) for the Antarctic ice sheet, and most recently by Morlighem et al. (2016) to model the evolution of a major Greenland outlet glacier. It has previously been applied to Iceland (Hubbard, 2006), the British Isles (Golledge et al., 2009; Hubbard et al., 2009; Kuchar et al., 2012; Patton et al., 2013) and Patagonia (Hubbard et al., 2005) to investigate the build-up, extent and deglaciation of the LGM ice sheets that occupied these regions. The approach adopted to solve the stress/strain field equates to the L1L2 classification of higher-order models defined by Hindmarsh (2004), and includes longitudinal (membrane) stresses. Including higher order stresses becomes increasingly important over steep terrain and/or under conditions of low basal traction. The model performs well in the ISMIP-HOM benchmark experiments when compared to second-order and full-Stokes schemes (Pattyn et al., 2008) and has been applied and validated against observations of 3D ice flow at Haut Glacier d'Arolla (Hubbard et al., 1998) and Glacier de Tsanfluron (Chandler et al., 2006; Hubbard et al., 2003) under complex ice rheologies.

Boundary conditions include: i) a present-day reference climate comprising monthly mean air temperature and precipitation, ii) basal topography, and iii) the geothermal heat flux. The model is integrated forward in time on a finite-difference grid with a resolution of 10 km through perturbations in temperature and eustatic sea-level. Gridded input and output is projected under an equal area Lambert Azimuthal projection, with a central meridian of 73°E. Common model parameters, constants, and values are presented in Supplementary Table 1. Model construction, assumptions and limitations are fully described in the references above; detailed description here is limited to where its implementation is specifically different from previous applications.

Surface mass balance

The mass balance of a glacier is determined as the difference between gains (accumulation) and losses (ablation), usually over one year. In simple terms, these net changes are dominated by precipitation and melting across the ice surface, and through the loss of icebergs at marine-terminating margins. In the model, surface mass balance is determined by a positive degree-day (PDD) scheme applied according to Laumann and Reeh (1993), and derives total melt from integrated monthly positive temperatures. Monthly temperature is calculated from the mean annual air temperature (MAAT) data, assuming a sinusoidal function with maximum and minimum peaks equating to mean monthly July and January temperatures. Cumulative PDDs for each month are calculated using a probability function based on a relationship between the standard deviation of daily to mean monthly temperature. Despite the limitations of such schemes (Golledge et al., 2010; Seguinot, 2013; van der Veen, 2002), their general ability to simulate glacier responses in contemporary Arctic environments (Braithwaite, 1995; De Woul and Hock, 2005; Jóhannesson et al., 1995) lends confidence in their use. Palaeo-climate forcing is implemented from the NGRIP $\delta^{18}O$ record (Andersen et al., 2004), that is linearly scaled between a maximum prescribed temperature depression and present-day conditions. Bulk precipitation is distributed evenly throughout the year and accumulates as snow when the surface temperature falls below a threshold of 1 °C. Winter expansion of sea ice across the North Atlantic probably impacted upon precipitation seasonality during stadial conditions, leading to a summer bias in the annual precipitation distribution across maritime sectors (Koenigk et al., 2009; Thomas et al., 2008). Annual precipitation totals were thus

likely greater than implied by the effective precipitation volumes recorded by glacier geometries here due to the increased losses from the system associated with summer rainfall (Golledge et al., 2010).

Spatial and temporal patterns of temperature and precipitation are dynamically coupled with the evolving ice sheet through applied temperature/precipitation – elevation (lapse-rate) relationships. These are derived from multiple-regression of meteorological data from the WorldClim database (Hijmans et al., 2005; Version 1.4) during the climatic reference period 1950 to 2000 (Supplementary Table 2). To account for the broad-scale variability between maritime conditions across western Europe and the continental climate of eastern Europe and northern Russia, the modelled climate is calculated across three prescribed sub-domains. Their extents are determined by the probable maximum extent and influence of each ice sheet, with a broad overlap given to avoid sharp climatic contrasts. Where transitions occur between sub domains, changes in climate parameters such as MAAT suppression and bulk precipitation are calculated assuming a linear gradient. Primary climate differences between these sub domains include a northwards decrease in temperature cooling and northwards increase in precipitation availability.

A limitation of the model is that we do not calculate the general circulation. Large-scale changes in climate related to shifts in atmospheric circulation are thus not accounted for, although broad scale distributions, for example rain shadow effects, can be incorporated manually by the application of linear gradients.

Independent variables used in regression analysis to determine the spatial distribution of temperature include easting, northing, latitude, longitude, elevation and (maritime) proximity to the North Atlantic thermohaline current. To determine the spatial pattern of the precipitation, an additional independent parameter - δ_{temp} - was used as a measure for continentality, being the residual between the summer and winter temperatures. R^2 values are typically >90% for temperature across all three climatic domains, indicating temperature distributions can be readily parameterised within the model. Precipitation for CIS and FIS sectors yield weaker correlations for the present-day distribution with a R^2 value of c. 60%, though the BSIS sector is better described with an R^2 value of 86% (Supplementary Table 2).

Sublimation is also incorporated into mass balance calculations in the High Arctic. Net water vapour fluxes to and from the ice sheet surface are important components of ablation in cold continental settings where humidity is low (Box et al., 2004; e.g., Fujii and Kusunoki, 1982; Kameda et al., 1997). A modelling study over the Greenland ice sheet revealed that these components can account for up to 12.5% (74 km^3 a^{-1}) net reduction in accumulation from snowfall (Ohmura et al., 1999). Field based studies provide confirmation of these model results with sublimation accounting for a 12-23% total precipitation loss (Box and Steffen, 2001). Across the Greenland ice sheet, sublimation is controlled by two factors – latitude, which is a proxy for the length and intensity of direct solar radiation, and elevation, since high-elevation sites generally have stronger temperature inversions and lower surface winds as katabatic winds tend to accelerate towards the coast as the surface slope angle increases. Sublimation is calculated based on a multiple regression analysis of these two *in situ* measurements from the Greenland Climate Network (GC-Net) (One level method: Box and Steffen, 2001). In the absence of more certain contributions of blowing snow sublimation rates on temporal and spatial trends of the surface mass balance (e.g., Déry and Yau, 2002), and for simplicity, calculated sublimation fluxes are applied evenly throughout the year.

Topography

Topographic and bathymetric datasets were melded from the International Bathymetric Chart of the Arctic Ocean (IBCAO) dataset (Jakobsson et al., 2012) above 60°N, and GEBCO_14

(http://www.gebco.net/) for areas south of 60°N. All topographic data were merged onto a custom Lambert Azimuthal equal-area projection and resampled to 10 km horizontal resolution using a nearest neighbour algorithm. Isostatic loading is implemented using an elastic lithosphere/relaxed asthenosphere scheme described by Le Meur and Huybrechts (1996) which provides a computationally pragmatic solution in the absence of a full spherical earth model.

Calving and basal dynamics

Calving losses at marine terminating margins are coupled to changing sea level (Waelbroeck et al., 2002) using a standard empirical function relating the calving flux (U_c) to ice thickness (H) and water depth, W_d (Brown et al., 1982; van der Veen, 1999). The sensitivity of calving to, for example, variations in ocean temperature (Luckman et al., 2015) and sea-ice buttressing (Hoff et al., 2016) can be controlled spatially and temporally through a variable calving coefficient, A_c (Hubbard, 2006) (Supplementary Table 1):

$$U_c = A_C H W_d \quad .$$

In the absence of explicit calculations of such external feedbacks, this depth-related calving coefficient provides a pragmatic and computationally efficient parameterisation for determining mass loss at marine terminating margins of the ice complex.

Basal sliding is determined by a Weertman (1964) sliding law, adjusted using an exponential decay function to initiate basal motion at sub pressure-melting temperatures (e.g., Fowler, 1986; Kleman et al., 1999; Wilch and Hughes, 2000). The sliding rate factor for temperatures, θ, ≤ 0.75 K below the pressure-melting point, A_s, is defined by:

$$A_s = A_s^0 \exp\left[-\gamma\,\theta_m - \theta\right],$$

where A_s^0 is the sliding rate factor at the pressure-melting point temperature, θ_m, and the coefficient γ is set to 1 K^{-1} (Hindmarsh and Le Meur, 2001). At 0.75 K below the pressure-melting point, sliding is 0.47 of its value at the pressure-melting point.

The model is applied to a 10 km finite-difference mesh with the inclusion of grounding-line dynamics based on the analytical boundary-treatment of Schoof (2007) and adapted in 2D by Pollard and DeConto (2007), which defines the ice flux at the grounding line as a function of ice thickness linearly interpolated between the adjacent node that bracket floating and grounded ice (Hubbard et al., 2009).

A spatially-variable distribution of geothermal heat flux is applied, interpolated onto the model domain from core measurements sourced from the Global Heat Flow Data Base (Pollack et al., 1993). While geothermal heat flux is largely dominated by low mean continental shield values close to 50 mW m^{-2} throughout Eurasia, several hotspots exist offshore of northern Finnmark, Norway, and eastern Svalbard.

Andersen, K.K., Azuma, N., Barnola, J.-M., Bigler, M., Biscaye, P., Caillon, N., Chappellaz, J., Clausen, H.B., Dahl-Jensen, D., Fischer, H., Flückiger, J., Fritzsche, D., Fujii, Y., Goto-Azuma, K., Grønvold, K., Gundestrup, N.S., Hansson, M., Huber, C., Hvidberg, C.S., Johnsen, S.J., Jonsell, U., Jouzel, J., Kipfstuhl, S., Landais, A., Leuenberger, M., Lorrain, R., Masson-Delmotte, V., Miller, H., Motoyama, H., Narita, H., Popp, T., Rasmussen, S.O., Raynaud, D., Rothlisberger, R., Ruth, U., Samyn, D., Schwander, J., Shoji, H., Siggard-Andersen, M.-L., Steffensen, J.P., Stocker, T., Sveinbjörnsdóttir, a E., Svensson, A., Takata, M., Tison, J.-L., Thorsteinsson, T., Watanabe, O., Wilhelms, F., White, J.W.C., 2004. High-resolution record of Northern Hemisphere climate extending into the last interglacial period. Nature 431, 147–151. doi:10.1038/nature02805

Blatter, H., 1995. Velocity and stress-fields in grounded glaciers - a simple algorithm for including deviatoric stress gradients. J. Glaciol. 41, 333–344. doi:10.3198/1995JoG41-138-333-344

Box, J.E., Bromwich, D.H., Bai, L., 2004. Greenland ice sheet surface mass balance 1991–2000: Application of Polar MM5 mesoscale model and in situ data. J. Geophys. Res. Atmos. 109, D16105. doi:10.1029/2003JD004451

Box, J.E., Steffen, K., 2001. Sublimation on the Greenland Ice Sheet from automated weather station observations. J. Geophys. Res. Atmos. 106, 33965–33981. doi:10.1029/2001JD900219

Braithwaite, R.J., 1995. Positive degree-day factors for ablation on the Greenland ice sheet studied by energy-balance modelling. J. Glaciol. 41, 153–160. doi:10.3198/1995JoG41-137-153-160

Brown, C.S., Meier, M.F., Post, A., 1982. Calving speed of Alaskan tidewater glaciers, with application to Columbia Glacier, US Geological Survey Professional Paper 1258-C.

Chandler, D.M., Hubbard, A.L., Hubbard, B.P., Nienow, P.W., 2006. A Monte Carlo error analysis for basal sliding velocity calculations. J. Geophys. Res. Earth Surf. 111, F04005. doi:10.1029/2006JF000476

De Woul, M., Hock, R., 2005. Static mass-balance sensitivity of Arctic glaciers and ice caps using a degree-day approach. Ann. Glaciol. 42, 217–224. doi:10.3189/172756405781813096

Déry, S.J., Yau, M.K., 2002. Large-scale mass balance effects of blowing snow and surface sublimation. J. Geophys. Res. Atmos. 107, ACL 8-1–ACL 8-17. doi:10.1029/2001JD001251

Fowler, A.C., 1986. Sub-temperate basal sliding. J. Glaciol. 32, 3–5. doi:10.3198/1986JoG32-110-3-5

Fujii, Y., Kusunoki, K., 1982. The role of sublimation and condensation in the formation of ice sheet surface at Mizuho Station, Antarctica. J. Geophys. Res. Ocean. 87, 4293–4300. doi:10.1029/JC087iC06p04293

Golledge, N., Hubbard, A., Bradwell, T., 2010. Influence of seasonality on glacier mass balance, and implications for palaeoclimate reconstructions. Clim. Dyn. 35, 757–770. doi:10.1007/s00382-009-0616-6

Golledge, N.R., Hubbard, A.L., Sugden, D.E., 2009. Mass balance, flow and subglacial processes of a modelled Younger Dryas ice cap in Scotland. J. Glaciol. 55, 32–42. doi:10.3189/002214309788608967

Hijmans, R.J., Cameron, S.E., Parra, J.L., Jones, P.G., Jarvis, A., 2005. Very high resolution interpolated climate surfaces for global land areas. Int. J. Climatol. 25, 1965–1978. doi:10.1002/joc.1276

Hindmarsh, R., Le Meur, E., 2001. Dynamical processes involved in the retreat of marine ice sheets. J. Glaciol. 47, 271–282. doi:10.3189/172756501781832269

Hindmarsh, R.C.A., 2004. A numerical comparison of approximations to the Stokes equations used in ice sheet and glacier modeling. J. Geophys. Res. Earth Surf. 109, F01012.

doi:10.1029/2003JF000065

Hubbard, A., 2006. The validation and sensitivity of a model of the Icelandic ice sheet. Quat. Sci. Rev. 25, 2297–2313. doi:10.1016/j.quascirev.2006.04.005

Hubbard, A., 2000. The verification and significance of three approaches to longitudinal stresses in high-resolution models of glacier flow. Geogr. Ann. Ser. A, Phys. Geogr. 82, 471–487. doi:10.1111/j.0435-3676.2000.00135.x

Hubbard, A., 1999. High-resolution modeling of the advance of the Younger Dryas ice sheet and its climate in Scotland. Quat. Res. 52, 27–43. doi:10.1006/qres.1999.2055

Hubbard, A., Blatter, H., Nienow, P., Mair, D., Hubbard, B., 1998. Comparison of a three-dimensional model for glacier flow with field data from Haut Glacier d'Arolla, Switzerland. J. Glaciol. 44, 368–378. doi:10.3198/1998JoG44-147-368-378

Hubbard, A., Bradwell, T., Golledge, N., Hall, A., Patton, H., Sugden, D., Cooper, R., Stoker, M., 2009. Dynamic cycles, ice streams and their impact on the extent, chronology and deglaciation of the British–Irish ice sheet. Quat. Sci. Rev. 28, 758–776. doi:10.1016/j.quascirev.2008.12.026

Hubbard, A., Hein, A.S., Kaplan Michael, R., Hulton, N.R.J., Glasser, N.F., 2005. A modelling reconstruction of the last glacial maximum ice sheet and its deglaciation in the vicinity of the Northern Patagonian Icefield, South America. Geogr. Ann. Ser. A, Phys. Geogr. 87, 375–391. doi:10.1111/j.0435-3676.2005.00264.x

Hubbard, B.P., Hubbard, A., Mader, H.M., Tison, J.-L., Grust, K., Nienow, P.W., 2003. Spatial variability in the water content and rheology of temperate glaciers: Glacier de Tsanfleuron, Switzerland. Ann. Glaciol. 37, 1–6. doi:10.3189/172756403781815474

Jakobsson, M., Mayer, L., Coakley, B., Dowdeswell, J.A., Forbes, S., Fridman, B., Hodnesdal, H., Noormets, R., Pedersen, R., Rebesco, M., Schenke, H.W., Zarayskaya, Y., Accettella, D., Armstrong, A., Anderson, R.M., Bienhoff, P., Camerlenghi, A., Church, I., Edwards, M., Gardner, J. V., Hall, J.K., Hell, B., Hestvik, O., Kristoffersen, Y., Marcussen, C., Mohammad, R., Mosher, D., Nghiem, S. V., Pedrosa, M.T., Travaglini, P.G., Weatherall, P., 2012. The International Bathymetric Chart of the Arctic Ocean (IBCAO) Version 3.0. Geophys. Res. Lett. 39, L12609. doi:10.1029/2012GL052219

Jóhannesson, T., Sigurdsson, O., Laumann, T., Kennett, M., 1995. Degree-day glacier mass-balance modelling with applications to glaciers in Iceland, Norway and Greenland. J. Glaciol. 41, 345–358. doi:10.3198/1995JoG41-138-345-358

Kameda, T., Azuma, N., Furukawa, T., Ageta, Y., Takahashi, S., 1997. Surface mass balance, sublimation and snow temperatures at Dome Fuji Station, Antarctica, in 1995. Proc. NIPR Symp. Polar Meteorol. Glaciol. 11, 24–34.

Kleman, J., Hättestrand, C., Clarhäll, A., 1999. Zooming in on frozen-bed patches: scale-dependent controls on Fennoscandian ice sheet basal thermal zonation. Ann. Glaciol. 28, 189–194. doi:10.3189/172756499781821670

Koenigk, T., Mikolajewicz, U., Jungclaus, J.H., Kroll, A., 2009. Sea ice in the Barents Sea: seasonal to interannual variability and climate feedbacks in a global coupled model. Clim. Dyn. 32, 1119–1138. doi:10.1007/s00382-008-0450-2

Kuchar, J., Milne, G., Hubbard, A., Patton, H., Bradley, S., Shennan, I., Edwards, R., 2012. Evaluation of a numerical model of the British-Irish ice sheet using relative sea-level data: implications for the interpretation of trimline observations. J. Quat. Sci. 27, 597–605. doi:10.1002/jqs.2552

Laumann, T., Reeh, N., 1993. Sensitivity to climate-change of the mass-balance of glaciers in southern

Norway. J. Glaciol. 39, 656–665. doi:10.3198/1993JoG39-133-656-665

Le Meur, E., Huybrechts, P., 1996. A comparison of different ways of dealing with isostasy: examples from modeling the Antarctic ice sheet during the last glacial cycle. Ann. Glaciol. 23, 309–317. doi:10.3198/1996AoG23-309-317

Luckman, A., Benn, D.I., Cottier, F., Bevan, S., Nilsen, F., Inall, M., 2015. Calving rates at tidewater glaciers vary strongly with ocean temperature. Nat. Commun. 6, 8566. doi:10.1038/ncomms9566

Marshall, S.J., Tarasov, L., Clarke, G.K.., Peltier, W.R., 2000. Glaciological reconstruction of the Laurentide Ice Sheet: physical processes and modelling challenges. Can. J. Earth Sci. 37, 769–793. doi:10.1139/e99-113

Morlighem, M., Bondzio, J., Seroussi, H., Rignot, E., Larour, E., Humbert, A., Rebuffi, S., 2016. Modeling of Store Gletscher's calving dynamics, West Greenland, in response to ocean thermal forcing. Geophys. Res. Lett. 43, 2659–2666. doi:10.1002/2016GL067695

Ohmura, A., Calanca, P., Wild, M., Anklin, M., 1999. Precipitation, accumulation and mass balance of the Greenland ice sheet. Zeitschrift fur Gletscherkd. und Glazialgeol. 31, 1–20.

Patton, H., Hubbard, A., Glasser, N.F., Bradwell, T., Golledge, N.R., 2013. The last Welsh Ice Cap: Part 1 - Modelling its evolution, sensitivity and associated climate. Boreas 42, 471–490. doi:10.1111/j.1502-3885.2012.00300.x

Pattyn, F., Perichon, L., Aschwanden, A., Breuer, B., de Smedt, B., Gagliardini, O., Gudmundsson, G.H., Hindmarsh, R.C.A., Hubbard, A., Johnson, J. V, Kleiner, T., Konovalov, Y., Martin, C., Payne, A.J., Pollard, D., Price, S., Rückamp, M., Saito, F., Souček, O., Sugiyama, S., Zwinger, T., 2008. Benchmark experiments for higher-order and full-Stokes ice sheet models (ISMIP–HOM). Cryosph. 2, 95–108. doi:10.5194/tc-2-95-2008

Pollack, H.N., Hurter, S.J., Johnson, J.R., 1993. Heat flow from the Earth's interior: Analysis of the global data set. Rev. Geophys. 31, 267. doi:10.1029/93RG01249

Pollard, D., DeConto, R.M., 2007. A coupled ice-sheet/ice-shelf/sediment model applied to a marine-margin flowline: forced and unforced variations., in: Hambrey, M.J., Christoffersen, P., Glasser, N.F., Hubbard, B. (Eds.), Glacial Sedimentary Processes and Products. Blackwell Publishing Ltd, Oxford.

Seguinot, J., 2013. Spatial and seasonal effects of temperature variability in a positive degree-day glacier surface mass-balance model. J. Glaciol. 59, 1202–1204. doi:10.3189/2013JoG13J081

Thomas, E.R., Mulvaney, R., Wolff, E.W., 2008. A change in seasonality in Greenland during a Dansgaard–Oeschger warming. Ann. Glaciol. 48, 19–24. doi:10.3189/172756408784700590

van der Veen, C.J., 2002. Polar ice sheets and global sea level: how well can we predict the future? Glob. Planet. Change 32, 165–194. doi:10.1016/S0921-8181(01)00140-0

van der Veen, C.J., 1999. Fundamentals of glacier dynamics. A.A. Balkema, Rotterdam.

Waelbroeck, C., Labeyrie, L., Michel, E., Duplessy, J.C., McManus, J.F., Lambeck, K., Balbon, E., Labracherie, M., 2002. Sea-level and deep water temperature changes derived from benthic foraminifera isotopic records. Quat. Sci. Rev. 21, 295–305. doi:10.1016/S0277-3791(01)00101-9

Weertman, J., 1964. The theory of glacier sliding. J. Glaciol. 5, 287–303.

Wilch, E., Hughes, T.J., 2000. Calculating basal thermal zones beneath the Antarctic ice sheet. J. Glaciol. 46, 297–310. doi:10.3189/172756500781832927

Parameter		Value	Units
g	Gravity	9.81	m s^{-2}
ρ	Density of ice	910	kg m^{-3}
ρ_w	Density of sea water	1028	kg m^{-3}
N	Glen flow-law exponent	3	
A_{weert}	Weertman sliding parameter	7.5 x 10^{-14}	
γ	Sub-melt sliding coefficient	1	K
m	Sliding-law exponent	1 – 3	
SF	Sliding factor	2.5	
A_s	Sliding-law coefficient	1.8 x 10^{-5}	m kPa^{-3} a^{-1}
A_0	Deformation enhancement	50	
a	Material constant		
	T^* < 263.15	1.14 x 10^{-5}	Pa^{-3} a^{-1}
	T^* ≥ 263.15	5.47 x 10^{10}	Pa^{-3} a^{-1}
Q	Creep activation energy		
	T^* < 263.15	60 x 10^3	J mol^{-1}
	T^* ≥ 263.15	139 x 10^3	J mol^{-1}
A_c	Calving parameter	1.07-29.4	a^{-1}
PDD_{ice}	PDD coefficient for ice	0.007	m °C m^{-1} d^{-1}
PDD_{snow}	PDD coefficient for snow	0.003	m °C m^{-1} d^{-1}
DDF	Degree day factor	0.005	
T	Temperature	-	K
T^*	(pressure melt corrected)	T – 8.7 x $10^{-4}H$	K
$T_{snow\text{-}rain}$	Snow-rain threshold	1.0	°C
R	Universal gas constant	8.314	J mol^{-1} K^{-1}
k_i	Thermal conductivity	2115.3 + 7.93 (T-273.15)	J m^{-1} K^{-1} a^{-1}
C_p	Specific heat capacity	3.1 x 10^8 exp(-0.0057T)	J kg^{-1} K^{-1} a^{-1}
φ	Internal frictional heating	-	J m^{-3} a^{-1}
G	Geothermal heat flux	15 – 705	mW m^{-2}
D	Flexural rigidity	5.0 x 10^{20}	N m
δt	Time step	0.0034	a
δx_i	Finite difference interval	1 x 10^4	m
	Central meridian	73	°E
	Latitude of origin	90	°N
x_{min}	Domain dimensions	-4750000	Lambert azimuthal equal area (central meridian 73°E)
x_{max}		1600000	
y_{min}		-3000000	
y_{max}		-190000	

STable 1: Principal parameters, constants and values used to force the ice-sheet model.

	Parameter	Celtic	Fenno-scandia	Barents Sea
Dependent:	**Summer temperature**			
	Intercept	10.75	3.578	1359
Independent:	Easting	-4.699E-5	-2.233E-5	3.093E-5
	Northing	2.37E-5	-7.497E-5	4.946E-5
	Latitude	*N/A*	*N/A*	-15.74
	Longitude	3.967	*N/A*	-0.5979
	Elevation	-4.766E-2	-5.179E-2	-3.692E-2
	Proximity	*N/A*	-4.843E-5	*N/A*
R^2 value		89.43%	89.67%	92.93%
Dependent:	**Winter temperature**			
	Intercept	-348	-102.2	44.49
Independent:	Easting	-7.211E-5	5.575E-5	2.382E-5
	Northing	*N/A*	8.791E-5	*N/A*
	Latitude	2.184	*N/A*	-2.004
	Elevation	-5.781E-2	-4.911E-2	-1.398
	Proximity	-2.296E-5	7.19E-5	-2.088E-5
R^2 value		92.2%	81.58%	96.0%
Dependent:	**Mean temperature**			
	Intercept	13.4	404.9	644.4
Independent:	Easting	-2.197E-5	-5.401E-6	-1.365E-5
	Northing	*N/A*	*N/A*	2.601E-5
	Latitude	-1.766	-5.823	-15.74
	Longitude	*N/A*	*N/A*	-0.5979
	Elevation	-5.294E-2	-4.994E-2	-3.692E-2
	Proximity	*N/A*	-2.166E-5	*N/A*
R^2 value		93.85%	93.85%	92.93%
Dependent:	**Annual precipitation**			
	Intercept	6717	2.528E4	2887
Independent:	Easting	6.6E-4	2.291E-3	1.521E-5
	Northing	-1.2E-3	*N/A*	8.751E-5
	Latitude	-58.94	-266.6	-31.07
	Longitude	-46.8	-37.92	-3.035
	Elevation	0.4682	0.1614	0.1076
	δtemp	-7.153	-3.926	-0.3889
	Proximity	-9.323E-4	-1.037E-3	9.847E-5
R^2 value		61.94%	60.17%	86.29%

STable 2: Parameters and R^2 values from multiple-regression analyses of climate across the model domain, detailing the ability of the model to reproduce present-day climate patterns utilising relatively few parameters. Eastings, northings and proximities are regressed in Lambert Azimuthal projection units (m), and elevation in m a.s.l.

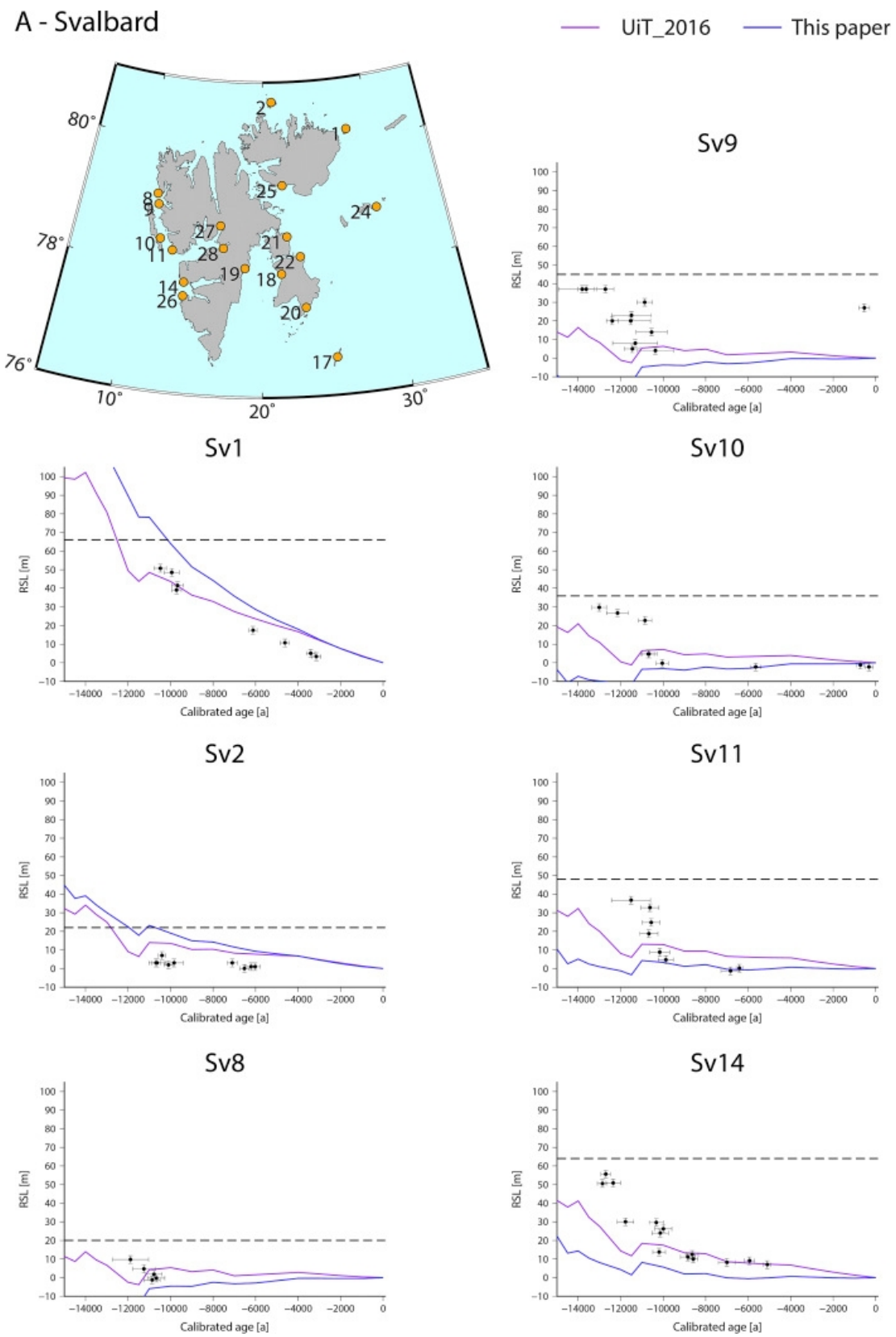

Supplementary Fig. S1. Comparisons between relative sea level (RSL) data and model predictions from this study (blue) for the four regions – A) Svalbard (Sv); B) Franz Josef Land (FJL); C) Novaya Zemlya (NZ); and D) northern Fennoscandia (Fe). The black symbols and error bars show the empirical observations, with the black dashed line giving the elevation of the highest marine limit. The UiT_2016 model data (pink) refers to an earlier published iteration of the modelled deglaciation wherein ice retreat was more loosely constrained (Auriac et al., 2016).

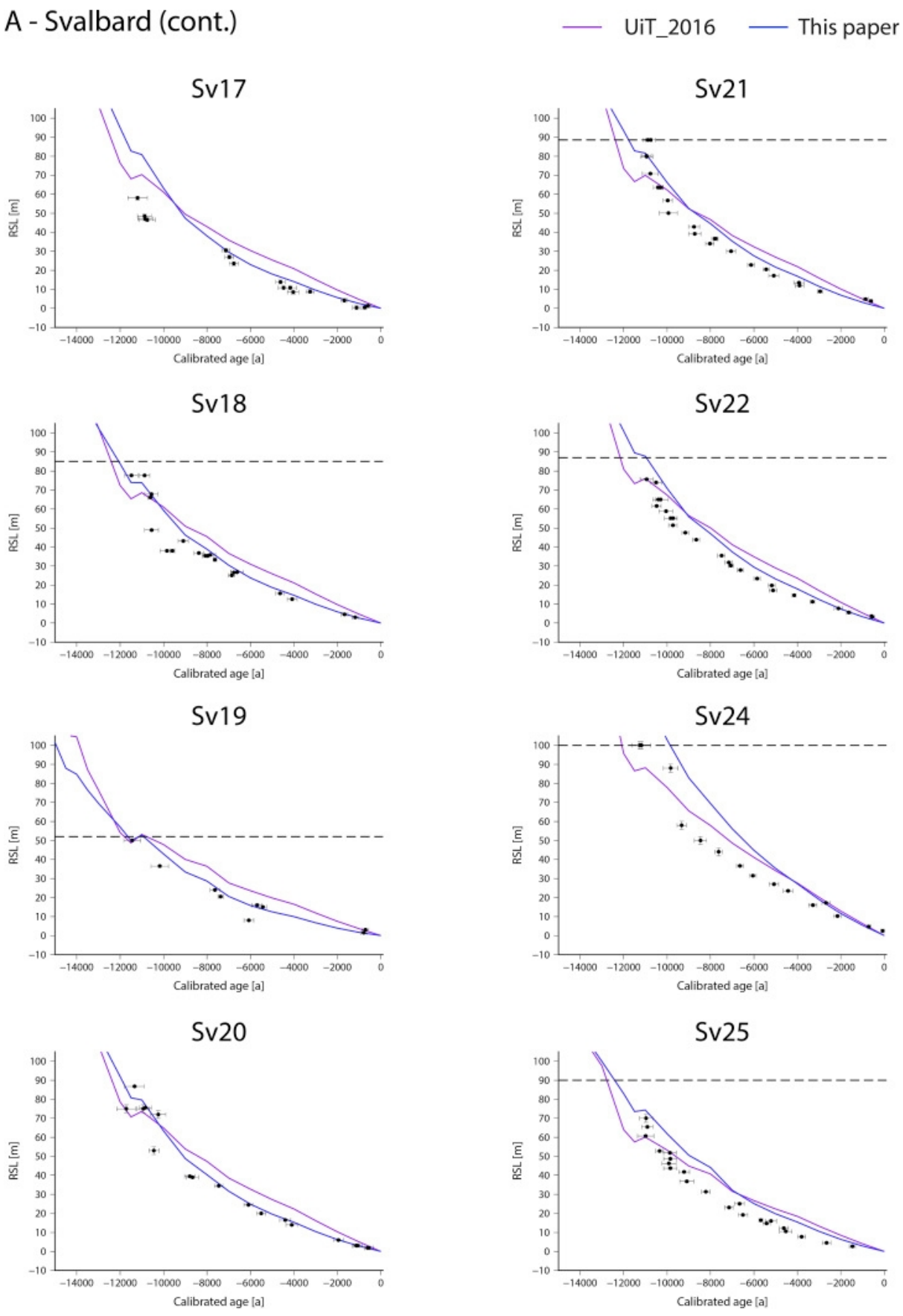

Supplementary Fig. S2.

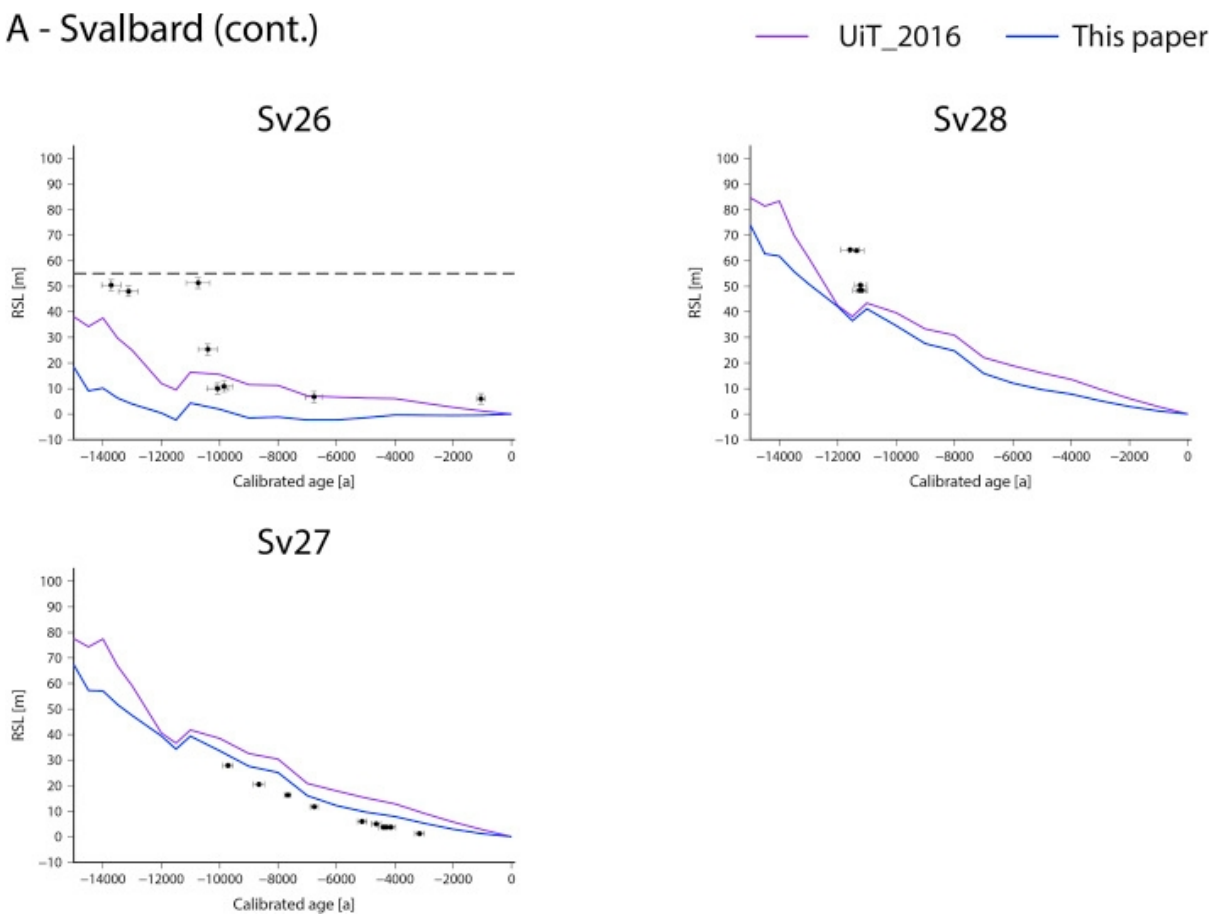

Supplementary Fig. S3.

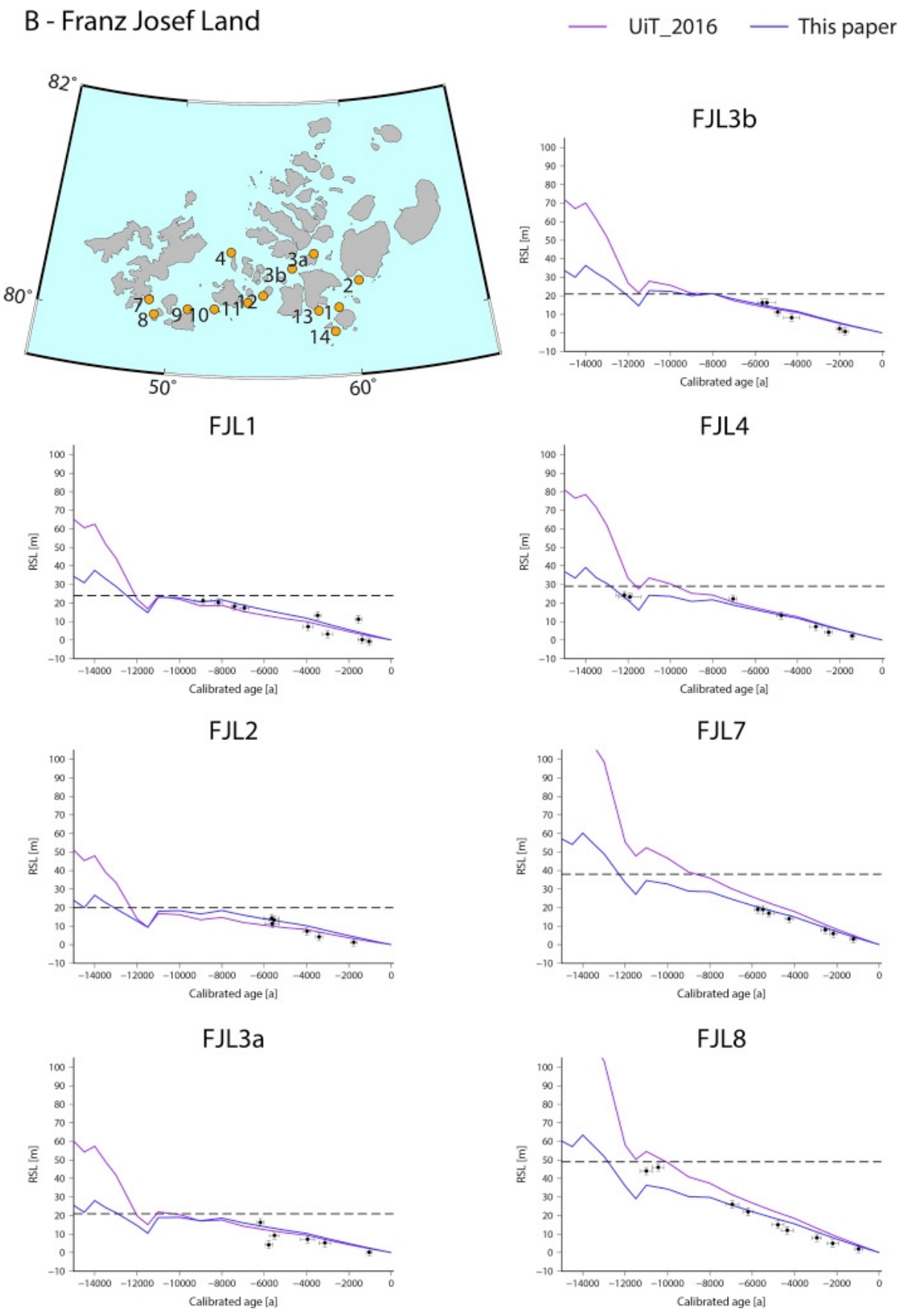

Supplementary Fig. S4.

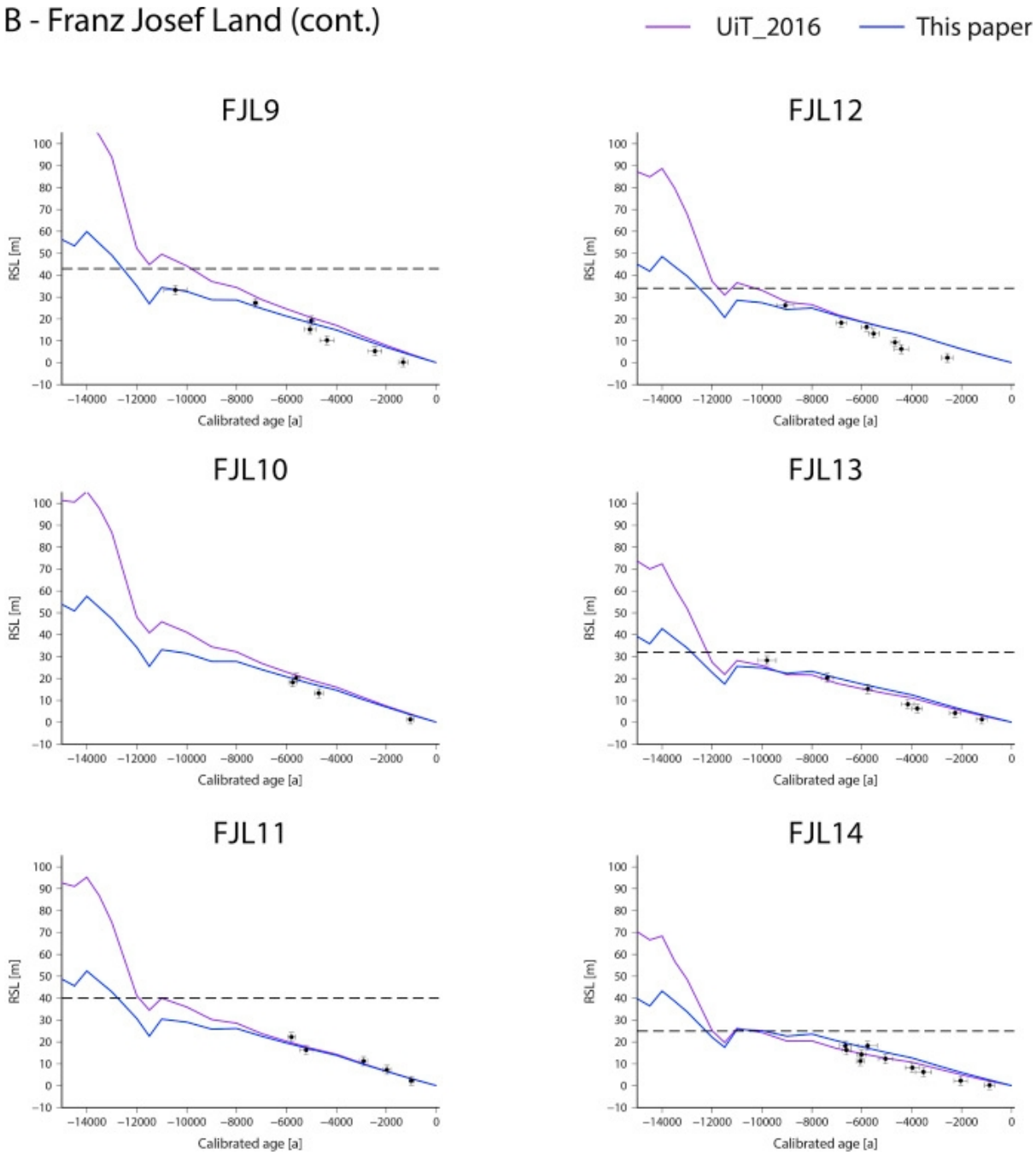

Supplementary Fig. S5.

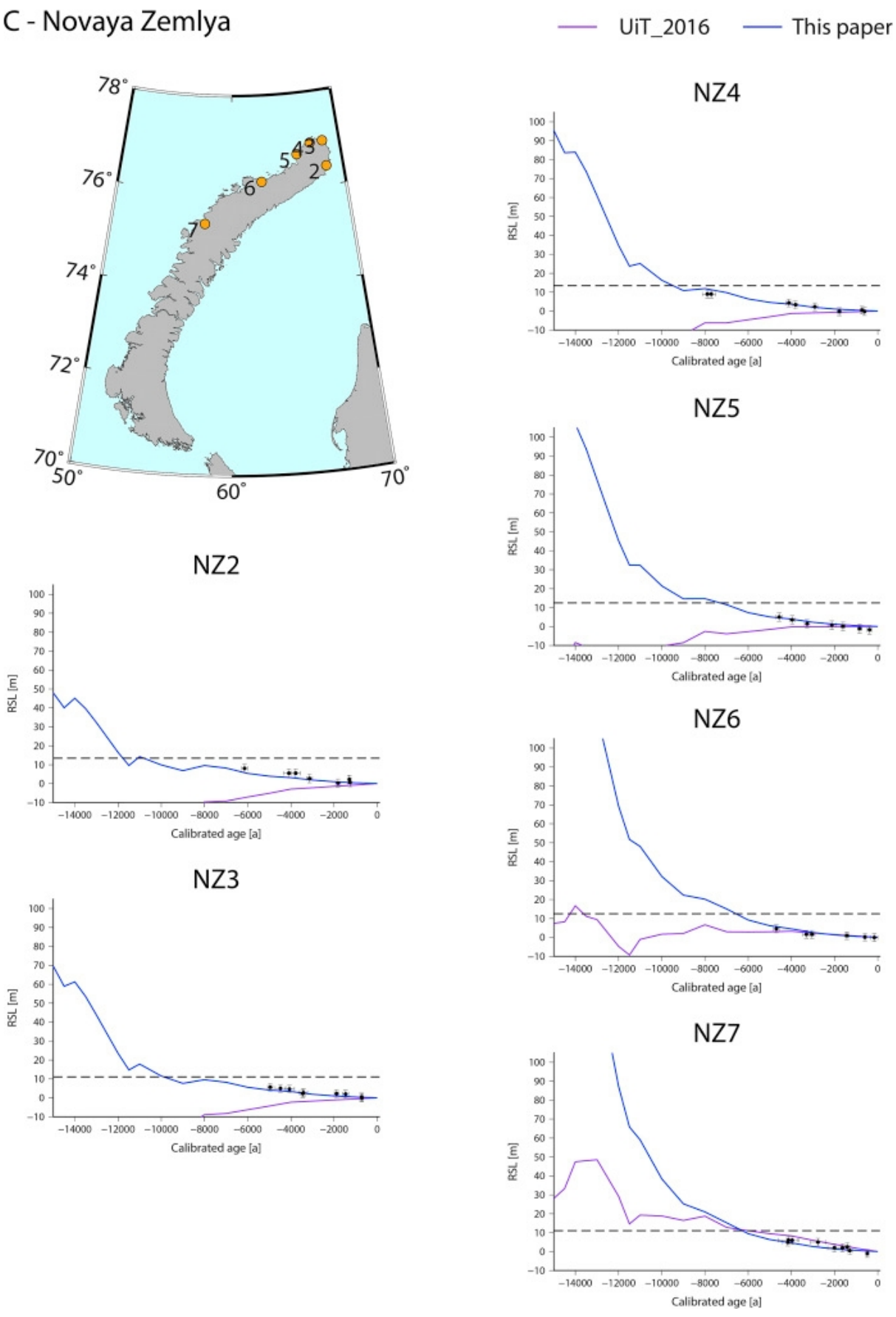

Supplementary Fig. S6.

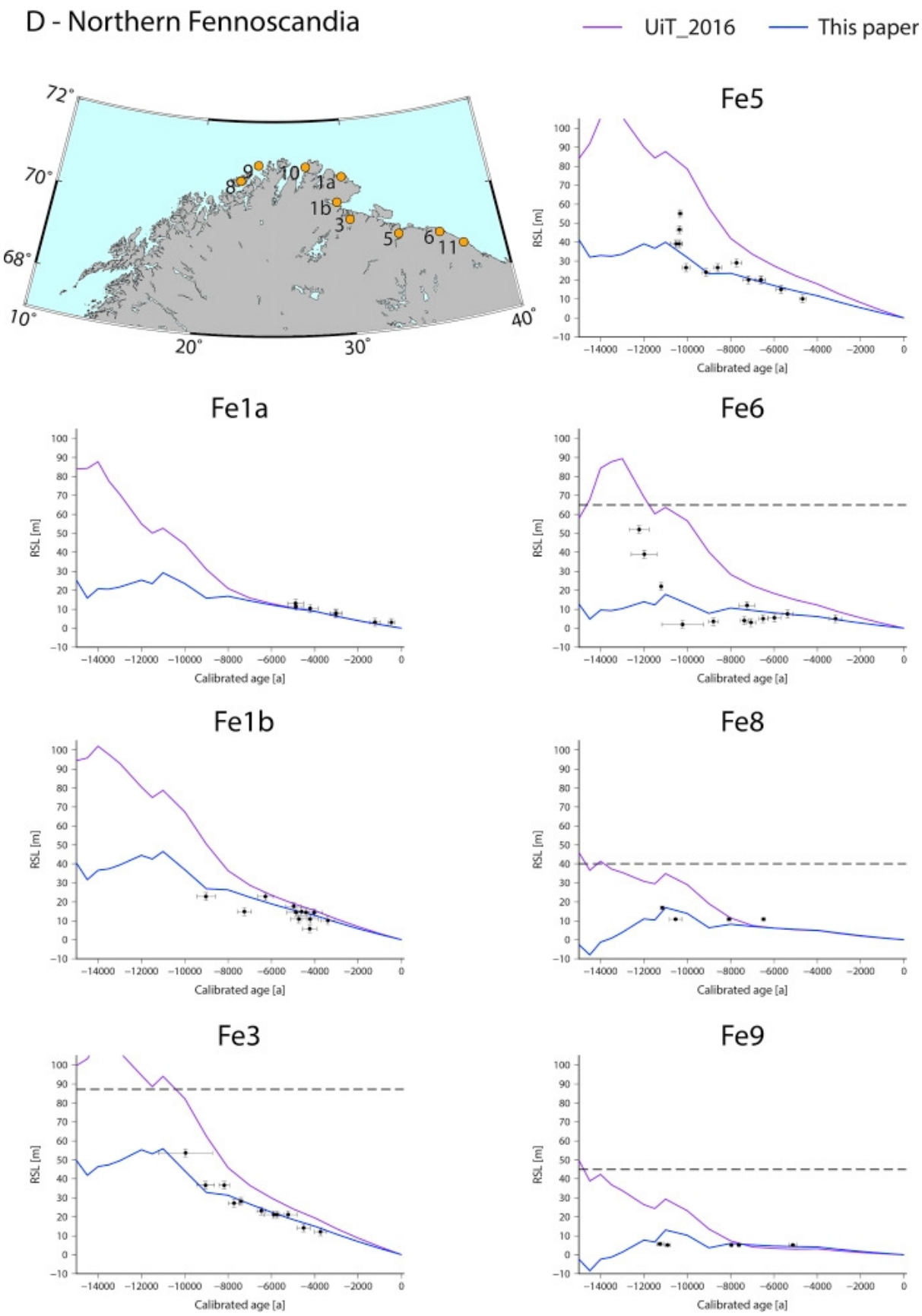

Supplementary Fig. S7.

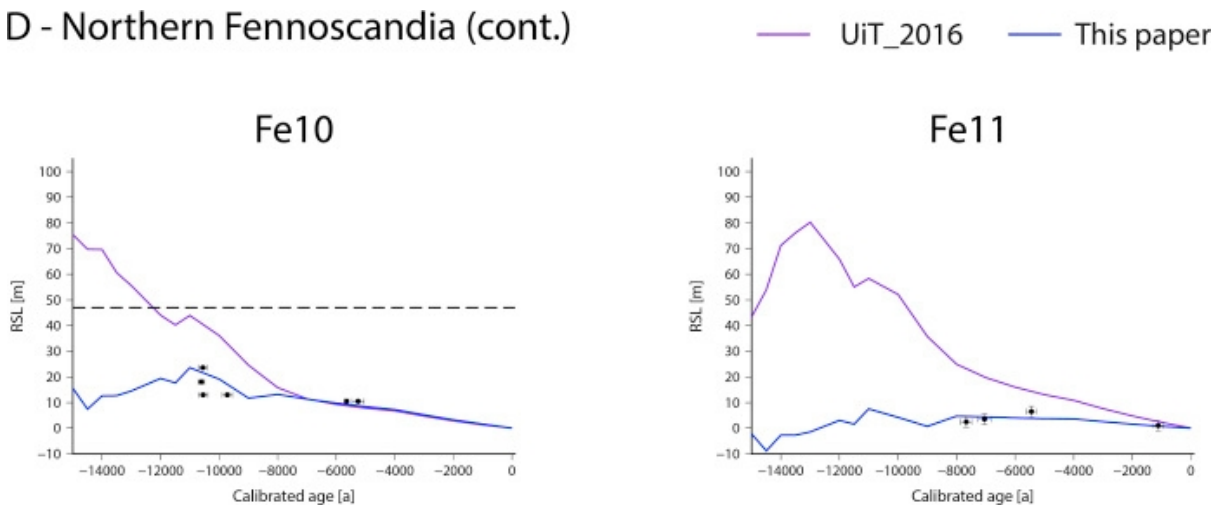

Supplementary Fig. S8.